CHEMISTRY OF MATERIALS
Article

Chem. Mater. **2009,** *21,* 3593–3601 3593
DOI:10.1021/cm901128j

Electronic Structure and Charge-Transport Parameters of Functionalized Tetracene Crystals: Impact of Partial Fluorination and Alkyl or Alkoxy Derivatization

Seyhan Salman, M. Carmen Ruiz Delgado,* Veaceslav Coropceanu, and Jean-Luc Brédas*

School of Chemistry and Biochemistry and Center for Organic Photonics and Electronics, Georgia Institute of Technology, Atlanta, Georgia 30332-0400

Received April 23, 2009. Revised Manuscript Received June 12, 2009

The charge-transport parameters of fluorine- and alkyl/alkoxy-substituted tetracene crystals have been investigated by means of density functional theory calculations. The intramolecular reorganization energy (vibronic coupling) is found to increase upon partial fluorination of tetracene and upon further alkoxy substitution, whereas alkyl substitution has a lesser impact. The calculated ionization energies are in agreement with electrochemical measurements and confirm that the electron injection barrier from conventional cathodes into partially fluorinated, alkyl/alkoxy-substituted tetracenes is expected to be smaller than into tetracene. Calculations of the intermolecular electronic couplings and of the crystal band structures have been performed to understand the role of packing on the charge-transport properties. A tight binding model with two sites per unit cell has been used to rationalize the results of the band-structure calculations. The largest electron mobility is predicted for the material where alkyl substitution of the partially fluorinated tetracene leads to a simple π-stacking motif; substitution resulting in dimerization along the π-stacks is found to significantly increase the charge-carrier effective mass and thus to adversely affect the carrier mobility.

1. Introduction

Conjugated organic materials have attracted much attention in recent years as they provide for a combination of the electrical and optical properties typical of semiconductors with properties such as flexibility, low cost, and structural tunability via chemical modification.[1−4] In particular, oligoacenes such as tetracene and pentacene have triggered interest as active components in (opto)electronic devices because of their high charge carrier mobilities.[5−11] However, shortcomings such as poor solubility or limited stability significantly weaken the viability of oligoacene-based devices. Therefore, many attempts have been made to enhance the charge-transport properties of the parent acenes via substitution or functionalization. For instance, Anthony and coworkers synthesized soluble and oxidatively stable pentacene derivatives through functionalization with bulky triisopropylsilylethynyl groups (TIPS-pentacene).[12] Fluorination is another extensively used strategy to tune the structural and electronic properties of organic semiconductors.[13−21] It was shown, for example, that partial fluorination enhances crystallization and stability of soluble antradithiophene semiconductors.[19] Partial fluorination can also trigger the formation of alternating face-to-face stacks[16] and reduce the interplanar spacing between acenes in the solid state;[17] this is generally considered to be a consequence of the electrostatic interactions

*Corresponding author. E-mail: maria.delgado@chemistry.gatech.edu (M.D.); jean-luc.bredas@chemistry.gatech.edu (J.-L.B.).

(1) Tang, C. W. *Appl. Phys. Lett.* **1986**, *48*, 183.
(2) Sariciftci, N. S.; Smilowitz, L.; Heeger, A. J.; Wudl, F. *Science* **1992**, *258*, 1474.
(3) Friend, R. H.; Gymer, R. W.; Holmes, A. B.; Burroughes, J. H.; Marks, R. N.; Taliani, C.; Bradley, D. D. C.; Dos Santos, D. A.; Brédas, J. L.; Logdlund, M.; Salaneck, W. R. *Nature* **1999**, *397*, 121.
(4) Bao, Z.; Locklin, J. *Organic Field-Effect Transistors*, 1st ed.; CRC Press: Boca Raton, FL, 2007.
(5) Karl, N.; Stehle, R.; Warta, W. *Mol. Cryst. Liq. Cryst.* **1985**, *120*, 247.
(6) Yamada, M.; Ikemoto, I.; Kuroda, H. *Bull. Chem. Soc. Jpn.* **1988**, *61*, 1057.
(7) Klauk, H.; Jackson, T. N. *Solid State Technol.* **2000**, *43*, 63.
(8) Klauk, H.; Halik, M.; Zschieschang, U.; Schmid, G.; Radlik, W.; Weber, W. *J. Appl. Phys.* **2002**, *92*, 5259.
(9) Jurchescu, O. D.; Baas, J.; Palstra, T. T. M. *Appl. Phys. Lett.* **2004**, *84*, 3061.
(10) Sundar, V. C.; Zaumseil, J.; Podzorov, V.; Menard, E.; Willett, R. L.; Someya, T.; Gershenson, M. E.; Rogers, J. A. *Science* **2004**, *303*, 1644.
(11) Fritz, S. E.; Martin, S. M.; Frisbie, C. D.; Ward, M. D.; Toney, M. F. *J. Am. Chem. Soc.* **2004**, *126*, 4084.
(12) Anthony, J. E.; Brooks, J. S.; Eaton, D. L.; Parkin, S. R. *J. Am. Chem. Soc.* **2001**, *123*, 9482.
(13) Sakamoto, Y.; Komatsu, S.; Suzuki, T. *J. Am. Chem. Soc.* **2001**, *123*, 4643.
(14) Facchetti, A.; Yoon, M. H.; Stern, C. L.; Katz, H. E.; Marks, T. J. *Angew. Chem., Int. Ed.* **2003**, *42*, 3900.
(15) Sakamoto, Y.; Suzuki, T.; Kobayashi, M.; Gao, Y.; Fukai, Y.; Inoue, Y.; Sato, F.; Tokito, S. *J. Am. Chem. Soc.* **2004**, *126*, 8138.
(16) Cho, D. M.; Parkin, S. R.; Watson, M. D. *Org. Lett.* **2005**, *7*, 1067.
(17) Swartz, C. R.; Parkin, S. R.; Bullock, J. E.; Anthony, J. E.; Mayer, A. C.; Malliaras, G. G. *Org. Lett.* **2005**, *7*, 3163.
(18) Chen, Z. H.; Muller, P.; Swager, T. M. *Org. Lett.* **2006**, *8*, 273.
(19) Subramanian, S.; Park, S. K.; Parkin, S. R.; Podzorov, V.; Jackson, T. N.; Anthony, J. E. *J. Am. Chem. Soc.* **2008**, *130*, 2706.
(20) Tang, M. L.; Reichardt, A. D.; Miyaki, N.; Stoltenberg, R. M.; Bao, Z. *J. Am. Chem. Soc.* **2008**, *130*, 6064.
(21) Tannaci, J. F.; Noji, M.; Mcbee, J. L.; Tilley, T. D. *J. Org. Chem.* **2008**, *73*, 7895.

Published on Web 07/20/2009

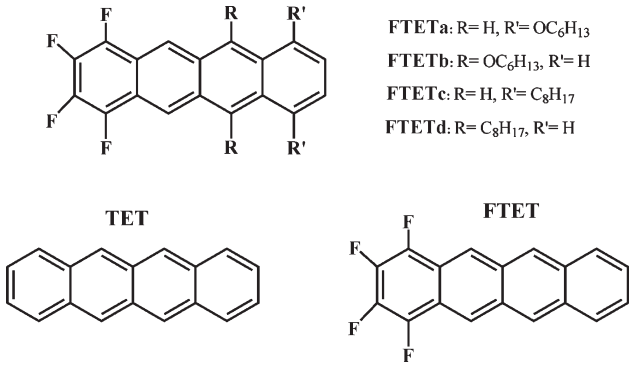

Figure 1. Chemical structures of the tetracenes examined in this study: (a) fluorine- and alkyl/alkoxy-functionalized tetracene derivatives (**FTETa-d**), (b) tetracene (**TET**), and (c) partially fluorinated tetracene (**FTET**).

between arenes (i.e., the center of the rings are electron-rich) and highly fluorinated arenes which feature an inverse electron density distribution (i.e., the center of the rings are electron-poor), also known as arene−perfluoroarene interactions.[22−24]

Recently, Swager and co-workers synthesized soluble and π-stacking tetracene derivatives[18] (Figure 1) by introducing on the one hand long alkyl or alkoxy side-chains in order to impart solubility and on the other hand partial fluorination to overcome herringbone packing in the solid state. In this work, we investigate the effect of functionalization and crystal packing on the electronic structure and charge-transport properties of these tetracene derivatives by means of density functional theory (DFT) calculations. To gain a better understanding of the role of partial fluorination and alkyl/alkoxy functionalization, the results for the substituted tetracenes **FTETa−d** are compared with those for unsubstituted tetracene (**TET**) and partially fluorinated tetracene (**FTET**).

2. Theoretical Methodology

The geometries of the neutral, cationic, and anionic states of the individual molecules were optimized at the DFT level by using the Becke-three-parameter Lee−Yang−Parr (B3LYP) hybrid density functional[25,26] and the 6-31G(d,p) basis set as implemented in the Gaussian 03 program package.[27] The long octyl or hexyloxy side chains were replaced with methyl or methoxy groups in order to reduce the computational cost. The same level of theory was used to derive the harmonic frequencies, reorganization energies, electron affinities (EA), and first ionization potentials (IP). The IP and EA energies are calculated by means of the ΔSCF procedure; both vertical and adiabatic quantities were derived from the differences in the ground-state energies of the neutral and charged molecules (in the vertical case, both states are taken at the optimal geometry of the neutral state; in the adiabatic case, both states are taken at their respective optimal geometries). Vertical one-electron excitations were computed using the time-dependent DFT (TDDFT) method.[28,29] TDDFT calculations were carried out using the B3LYP functional and the 6-31G(d,p) basis set on the previously optimized molecular geometries obtained at the same level of theory.

The calculations of the electronic band structures of the fluorinated tetracenes **FTETa-d** were performed with the CRYSTAL06 program.[30] The B3LYP functional and the 6-31G basis set were used with a uniform $6 \times 6 \times 6$ Monkhorst-Pack k-point mesh.[31] In the case of the (more asymmetric) **FTETc** crystal, the band-structure calculations were also performed with a $10 \times 6 \times 2$ k-point mesh. In addition, following the basis set orthogonalization procedure described recently,[32] the transfer integrals (electronic couplings) between adjacent monomers (extracted from the crystal structure geometry) were calculated using the PW91 functional and the triple-ξ plus polarization (TZP) basis set as implemented in the ADF program package.[33]

3. Results and Discussion

3.1. Geometric Structure. The geometry modifications occurring upon oxidation and reduction in the substituted tetracenes and the parent **TET** and **FTET** molecules are listed in Tables 1 and 2, respectively (the optimized geometries of the molecules in their neutral, radical-anion, and radical-cation states are collected in the Supporting Information, see Tables S1−S6). The DFT bond lengths for the neutral states of **FTETa−d** are in good agreement with the experimental crystal data.[18] The calculations show that although most of the geometrical changes upon oxidation/reduction of **TET** take place within the C−C bonds along the whole molecular periphery, in the case of **FTETa−d**, the main geometrical modifications occur on the substituted benzene rings. These results parallel the asymmetry in charge distribution along the tetracene backbone (and resulting molecular dipole moments, see Table S7 in the Supporting Information) induced by the incorporation of both

(22) Williams, J. H. *Acc. Chem. Res.* **1993**, *26*, 593.
(23) Meyer, E. A.; Castellano, R. K.; Diederich, F. *Angew. Chem., Int. Ed.* **2003**, *42*, 1210.
(24) Reichenbacher, K.; Suss, H. I.; Hulliger, J. *Chem. Soc. Rev.* **2005**, *34*, 22.
(25) Becke, A. D. *J. Chem. Phys.* **1993**, *98*, 5648.
(26) Lee, C. T.; Yang, W. T.; Parr, R. G. *Phys. Rev. B* **1988**, *37*, 785.
(27) Frisch, M. J.; , Trucks, G. W.; Schlegel, H. B.; Scuseria, G. E.; Robb, M. A.; Cheeseman, J. R.; Montgomery, J. A., Jr.; Vreven, T.; Kudin, K. N.; , Burant, J. C.; Millam, J. M.; Iyengar, S. S.; Tomasi, J.; Barone, V.; Mennucci, B.; Cossi, M.; Scalmani, G.; Rega, N.; Petersson, G. A.; Nakatsuji, H.; Hada, M.; Ehara, M.; Toyota, K.; Fukuda, R.; Hasegawa, J.; Ishida, M.; Nakajima, T.; Honda, Y.; Kitao, O.; Nakai, H.; Klene, M.; Li, X.; Knox, J. E.; Hratchian, H. P.; Cross, J. B.; Adamo, C.; Jaramillo, J.; Gomperts, R.; Stratmann, R. E.; Yazyev, O.; Austin, A. J.; Cammi, R.; Pomelli, C.; Ochterski, J. W.; Ayala, P. Y.; Morokuma, K.; Voth, G. A.; Salvador, P.; Dannenberg, J. J.; Zakrzewski, V. G.; Dapprich, S.; Daniels, A. D.; Strain, M. C.; Farkas, O.; Malick, D. K.; Rabuck, A. D.; Raghavachari, K.; Foresman, J. B.; Ortiz, J. V.; Cui, Q.; Baboul, A. G.; Clifford, S.; Cioslowski, J.; Stefanov, B. B.; Liu, G.; Liashenko, A.; Piskorz, P.; Komaromi, I.; Marin, R. L.; Fox, D. J.; Keith, T.; Al-Laham, M. A.; Peng, C. Y.; Nanayakkara, A.; Challacombe, M.; Gill, P. M. W.; Johnson, B.; Chen, W.; Wong, M. W.; Gonzalez, C.; Pople, J. A. *Gaussian 03, Revision B.02*; Gaussian, Inc.: Pittsburgh PA, 2003.
(28) Runge, E.; Gross, E. K. U. *Phys. Rev. Lett.* **1984**, *52*, 997.
(29) Gross, E. K. U.; Driezler, R. M. *Density Functional Theory*; Plenum Press: New York, 1995.
(30) Dovesi, R.; Saunders, V. R.; Roetti, C.; Orlando, R.; Zicovich-Wilson, C. M.; Pascale, F.; Civalleri, B.; Doll, K.; Harrison, N. M.; Bush, I. J.; D'Arco, P.; Llunell, M. *CRYSTAL06*; University of Torino: Torino, Italy, 2006.
(31) Monkhorst, H. J.; Pack, J. D. *Phys. Rev. B* **1976**, *13*, 5188.
(32) Valeev, E. F.; Coropceanu, V.; da Silva, D. A.; Salman, S.; Brédas, J. L. *J. Am. Chem. Soc.* **2006**, *128*, 9882.
(33) Velde, G. T.; Bickelhaupt, F. M.; Baerends, E. J.; Guerra, C. F.; Van Gisbergen, S. J. A.; Snijders, J. G.; Ziegler, T. *J. Comput. Chem.* **2001**, *22*, 931.

Table 1. B3LYP/6-31G(d,p) Calculated Bond Length Changes (in Å) upon Oxidation (going from the neutral to the cation state) in Functionalized Tetracenes FTETa-d, TET, and FTET[a]

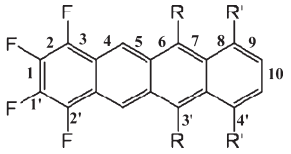

bonds	FTETa	FTETb	FTETc	FTETd	TET	FTET
1	−0.009	−0.013	−0.015	−0.013	−0.016	−0.016
2	0.013	0.017	0.019	0.018	0.015	0.021
3	−0.011	−0.013	−0.013	−0.013	−0.014	−0.014
4	0.010	0.013	0.013	0.011	0.014	0.013
5	−0.007	−0.009	−0.006	−0.006	−0.004	−0.005
6	0.002	0.005	−0.002	0.000	−0.004	−0.003
7	0.004	**0.022**	0.010	**0.020**	0.014	0.013
8	−0.008	−0.016	−0.014	−0.018	−0.014	−0.015
9	**0.030**	0.015	**0.020**	0.016	0.015	0.015
10	**−0.032**	−0.017	**−0.020**	−0.016	−0.016	−0.015
1′	−0.014	−0.015	−0.015	−0.016	−0.001	−0.016
2′	−0.011	−0.013	−0.014	−0.014	−0.001	−0.015
3′	0.000	**−0.029**	0.000	−0.006	−0.001	0.000
4′	**-0.030**	−0.001	−0.002	0.000	−0.001	−0.001

[a] The largest geometrical changes are highlighted in bold.

Table 2. B3LYP/6-31G(d,p) Calculated Bond Length Changes (in Å) upon Reduction (going from the neutral to the anion state) in Functionalized Tetracenes FTETa-d, TET, and FTET[a]

bonds	FTETa	FTETb	FETc	FTETd	TET	FTET
1	**−0.023**	**−0.022**	**−0.022**	**−0.021**	**−0.018**	**−0.022**
2	0.017	0.016	0.016	0.016	0.018	0.016
3	−0.014	−0.014	−0.014	−0.013	−0.011	−0.013
4	0.017	0.017	0.016	0.016	0.016	0.017
5	0.003	0.002	0.003	0.003	0.000	0.002
6	−0.003	−0.006	−0.003	−0.006	0.000	−0.003
7	0.019	0.013	0.018	0.017	0.016	0.017
8	−0.013	−0.012	−0.014	−0.013	−0.011	−0.012
9	0.011	0.017	0.016	0.018	0.018	0.017
10	−0.010	−0.017	−0.017	−0.017	−0.018	−0.018
1′	0.017	0.016	0.017	0.016	0.002	0.017
2′	0.016	0.015	0.016	0.014	0.002	0.016
3′	0.001	**0.019**	0.001	−0.001	0.001	0.002
4′	**0.019**	0.001	0.001	0.003	0.002	0.002

[a] The largest geometrical changes are highlighted in bold.

electron-donating and -withdrawing substituents onto the parent molecule. **FTETa** presents the biggest dipole moment in the series (about 6.2 D) and also undergoes the most significant structural change upon going from the neutral to the cationic state; the largest C−C bond length evolution is around 0.032 Å in **FTETa** and decreases to 0.029 Å for **FTETb** and 0.020 Å for **FTETc** and **FTETd**.

Upon oxidation, the largest geometrical modifications in **FTETa** and **FTETb** occur in the C−O bonds (bonds 4′ and 3′ for **FTETa** and **FTETb**, respectively). On the other hand, reduction of **FTETa−d** brings the largest C−C bond length changes along the fluorinated ring; significant geometrical evolutions of the C−O bonds (0.019 Å) are also observed in the alkoxy side chains of **FTETa** and **FTETb**, although less pronounced than those observed upon oxidation. The C−F bonds present similar geometric relaxations (bonds 1′ and 2′) upon oxidation and reduction within the **FTETa−d** series and **FTET**.

Table 3. B3LYP/6-31G(d,p) Estimates of the Reorganization Energy λ (in meV) for Hole-Transfer (HT) and Electron-Transfer (ET) Processes for FTETa−d, TET, and FTET

compd	λ(HT)	λ(ET)
FTETa	267	242
FTETb	264	239
FTETc	159	208
FTETd	195	208
TET	108	157
FTET	160	205

3.2. Reorganization Energies, Electron Affinities, and Ionization Potentials. The reorganization energy, λ, measures the strength of the so-called local electron−phonon coupling;[34] the smaller λ, the larger the expected charge mobility. It consists of both intra- and intermolecular contributions; the former reflects the changes in the geometry of individual molecules and the latter in the polarization of the surrounding molecules, upon going from the neutral to the charged state and vice versa. Here, we focus on the intramolecular contribution to λ as the nuclear polarization contribution is expected to be significantly smaller.[35] The DFT reorganization energies are collected in Table 3. The λ values in the **FTETa−d** compounds are in the range of 160−270 meV for hole transfer (HT); this is two-to-three times larger than the value calculated for pentacene, 95 meV,[36] and the value estimated both experimentally and theoretically for TIPS-pentacene (6,13-bis (triisopropylsilylethynyl) pentacene), 111 meV.[37] Interestingly, the lowest value of λ(HT) of 159 meV obtained in **FTETc** coincides with that calculated for rubrene.[38] For electron transfer (ET), the calculated λ values in **FTETa−d** (200−240 meV) are on the same order as that found for other organic systems considered as good electron-transport materials, such as perfluoropentacene[39] and *N*,*N*'-dipentyl-3,4,9,10-perylene tetracarboxylic diimide,[40] with values of 222 and 272 meV, respectively. The reorganization energies in the functionalized tetracenes studied here are signifi cantly larger (by ca. 100% and 40% for HT and ET, respectively) than in unsubstituted tetracene **TET** (108 meV for HT and 157 meV for ET). Among the series, the largest reorganization energies are found for the alkoxy-substituted system **FTETa** (267 meV for holes and 242 meV for electrons), which is consistent with the large geometric modifications upon ionization discussed above; **FTETc** has the smallest λ for both HT (159 meV)

(34) Coropceanu, V.; Cornil, J.; da Silva, D. A.; Olivier, Y.; Silbey, R.; Brédas, J. L. *Chem. Rev.* **2007**, *107*, 926.
(35) Norton, J. E.; Brédas, J. L. *J. Am. Chem. Soc.* **2008**, *130*, 12377.
(36) Malagoli, M.; Coropceanu, V.; da Silva, D. A.; Bredas, J. L. *J. Chem. Phys.* **2004**, *120*, 7490.
(37) Griffith, O. L.; Gruhn, N. E.; Anthony, J. E.; Purushothaman, B.; Lichtenberger, D. L. *J. Phys. Chem. C* **2008**, *112*, 20518.
(38) da Silva, D. A.; Kim, E. G.; Bredas, J. L. *Adv. Mater.* **2005**, *17*, 1072.
(39) Delgado, M. C. R.; Pigg, K. R.; Filho, D. A.d. S.; Gruhn, N. E.; Sakamoto, Y.; Suzuki, T.; Osuna, R. M.; Casado, J.; Hernández, V.; Navarrete, J. T. L.; Nortinelli, N.; Cornil, J.; Coropceanu, V.; Sánchez-Carrera, R. S.; Brédas, J. L. *J. Am. Chem. Soc.* **2009**, *131*, 1502.
(40) Chesterfield, R. J.; McKeen, J. C.; Newman, C. R.; Ewbank, P. C.; da Silva, D. A.; Bredas, J. L.; Miller, L. L.; Mann, K. R.; Frisbie, C. D. *J. Phys. Chem. B* **2004**, *108*, 19281.

Table 4. B3LYP/6-31G(d,p) HOMO and LUMO Energies along with the Experimental Optical Transition (E_{op}) and Computed TDDFT Energies (E_{TDDFT}) of the $S_0 \rightarrow S_1$ Transitions, for FTETa−d, TET, and FTET (all values are given in eV)

compd	HOMO	LUMO	Δ(HOMO−LUMO)	E_{TDDFT}[a]	E_{op}[b]
FTETa	−4.89	−2.22	2.67	2.30	2.25
FTETb	−5.06	−2.42	2.64	2.34	2.34
FTETc	−5.16	−2.39	2.77	2.46	2.47
FTETd	−5.07	−2.40	2.67	2.38	2.40
TET	−4.87	−2.09	2.78	2.49	2.57
FTET	−5.23	−2.47	2.76	2.47	-

[a] TDDFT/B3LYP/6-31G(d,p) vertical $S_0 \rightarrow S_1$ electronic transitions dominated by promotion of an electron from HOMO to LUMO. [b] Calculated from the onset of UV absorbance spectra measured in CH_2Cl_2 solution (ref 18).

and ET (208 meV), with values essentially identical to those calculated for **FTET**. The DFT calculations show that the λ values for alkoxy-substituted compounds **FTETa−b** are larger than for alkyl-substituted systems **FTETc−d**; this is consistent with the observed significant geometrical changes in the C−O bonds of the alkoxy side chains upon ionization of **FTETa−b**.

It is interesting to note that on a relative basis, the substitutions considered here impact the reorganization energy for electron transfer to a much smaller extent than for hole transfer (the increase from **TET** to **FTETa-b** is on the order of 50% in the former case and about 250% in the latter); λ(ET) even becomes slightly smaller than λ(HT) in **FTETa−b**.

The energies of the frontier orbitals are collected in Table 4. Partial fluorination stabilizes both the HOMO and LUMO (in a similar way) due to the strong inductive electron withdrawing effect of fluorine. On the other hand, the introduction of alkyl and alkoxy groups to **FTET**, because of the electron-donating ability of these side chains, results in the destabilization of the frontier molecular orbitals. The combination of these effects leads to HOMO and LUMO energies in **FTETa−d** that lie in between those of **TET** and **FTET**. Both the calculated HOMO−LUMO gaps and the TDDFT energies of the vertical $S_0 \rightarrow S_1$ electronic transitions (which essentially correspond to HOMO−LUMO single excitations) reproduce the decrease in experimental optical transition energy upon donor/acceptor substitution of **TET**. Within the **FTETa-d** series, the TDDFT $S_0 \rightarrow S_1$ transition energies provide an excellent agreement with the experimental optical transitions measured from the onset of the UV absorbance spectra; for instance, TDDFT yields the largest [smallest] optical transition for **FTETc** [**FTETa**] with a value of 2.46 [2.30] eV, which matches well the experimental value observed at 2.47 [2.25] eV.[18]

Vertical and adiabatic ionization potentials and electron affinities derived from ΔSCF calculations are given in Table 5. Upon going from **TET** to **FTET**, the ionization potentials increase by 0.3−0.4 eV. However, further inclusion of alkyl or alkoxy side chains into **FTET** contributes to decrease the ionization potentials by 0.1−0.5 eV, with the alkoxy groups having expectedly a larger impact than the alkyl groups; as a result, **FTETc−d** have relatively higher ionization potentials than **FTETa−b**,

Table 5. B3LYP/6-31G(d,p) First Ionization Potentials (IPs) and Electron Affinities (EAs) for FTETa−d, TET, and FTET, As Obtained from ΔSCF Calculations

	IP (eV)		EA (eV)	
compd	vertical	adiabatic	vertical	Adiabatic
FTETa	6.28	6.15	−0.79	−0.91
FTETb	6.47	6.34	−1.01	−1.13
FTETc	6.57	6.49	−0.96	−1.06
FTETd	6.49	6.39	−0.98	−1.09
TET	6.34	6.28	−0.63	−0.71
FTET	6.69	6.61	−1.00	−1.11

Table 6. Crystallographic Parameters for the Unit Cells of the Fluorinated Tetracenes FTETa-d[18]

	a (Å)	*b* (Å)	*c* (Å)	α (deg)	*β* (deg)	*γ* (deg)
FTETa	7.162	13.263	13.455	94.215	100.102	96.192
FTETb	7.547	11.965	14.843	79.330	82.968	79.947
FTETc	4.946	9.748	28.705	92.905	93.547	92.621
FTETd	7.951	16.883	22.692	107.104	99.040	102.780

which is consistent with the electrochemical measurements (the oxidation potentials of **FTETc** and **FTETd** are 0.56 and 0.48 V with respect to a Pt electrode, whereas those for **FTETa** and **FTETb** are 0.31 and 0.44 V, respectively).[18] The electron affinities become more exothermic upon partial fluorination (the **FTET** electron affinity is about 0.4 eV more exothermic than in **TET**) and with the exception of **FTETb** get reduced with introduction of the alkyl/alkoxy substituents. Overall, fluorination has a greater impact than alkyl/alkoxy substitution and tetracenes **FTETa−d** have more exothermic EAs than **TET**. The DFT results are supported by the electrochemical measurements which show that **FTETa−d** present reduction potentials between −1.84 and −1.92 V with respect to a Pt electrode, to be compared to −2.05 V in **TET**.[18] Thus, in comparison to tetracene, our results suggest that partially fluorinated, alkyl/alkoxy-substituted tetracenes are expected to reduce the electron injection barrier from low work−function electrodes in organic electronic devices.

3.3. Electronic Structure of the Crystals. The crystalline structures of **FTETa−d** belong to the triclinic ($P\bar{1}$) space group and are characterized by the lattice parameters given in Table 6. Interestingly, the molecules in all four structures are arranged into π-stacks in a slipped cofacial manner; this is in marked contrast to the herringbone packing motif of the parent tetracene crystal.[41]

The unit cells of **FTETa** and **FTETb** contain two translationally inequivalent molecules and present two alternating intermolecular distances between adjacent molecules along the π-stacks; the two related dimers are labeled in Figure 2 as a- and b-type. The intermolecular distances in **FTETa** and **FTETb** are 3.22 and 3.44 Å in the a-dimer, and 3.24 and 3.53 Å in the b-dimer, respectively.[18] It is also interesting to note that in the case of **FTETa** the alkoxy groups appear in a "cis-like" configuration in the a-dimer (i.e., facing each other) and in an "anti" configuration in the b-dimer. As seen from Figure 2, **FTETa** and **FTETb** form antiparallel π-stacks

(41) Robertson, J.; Trotter, J.; Sinclair, V. C. *Acta Crystallogr.* **1961**, *14*, 697.

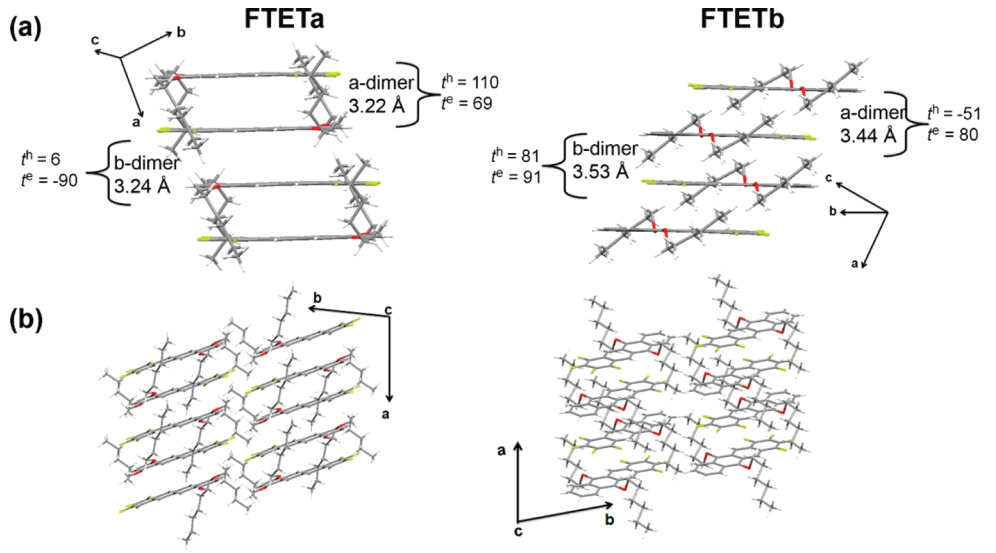

Figure 2. (a) Crystal packing (view along the short axis) of **FTETa** (left) and **FTETb** (right) showing the intermolecular distances within the a- and b-type dimers as given in ref 18. The DFT-estimates of the transfer integrals (in meV) for holes (t^h) and electrons (t^e) for these molecular pairs are also shown. (b) Crystal structure of **FTETa** (left) and **FTETb** (right) viewed along the *c* direction of the crystal lattice.

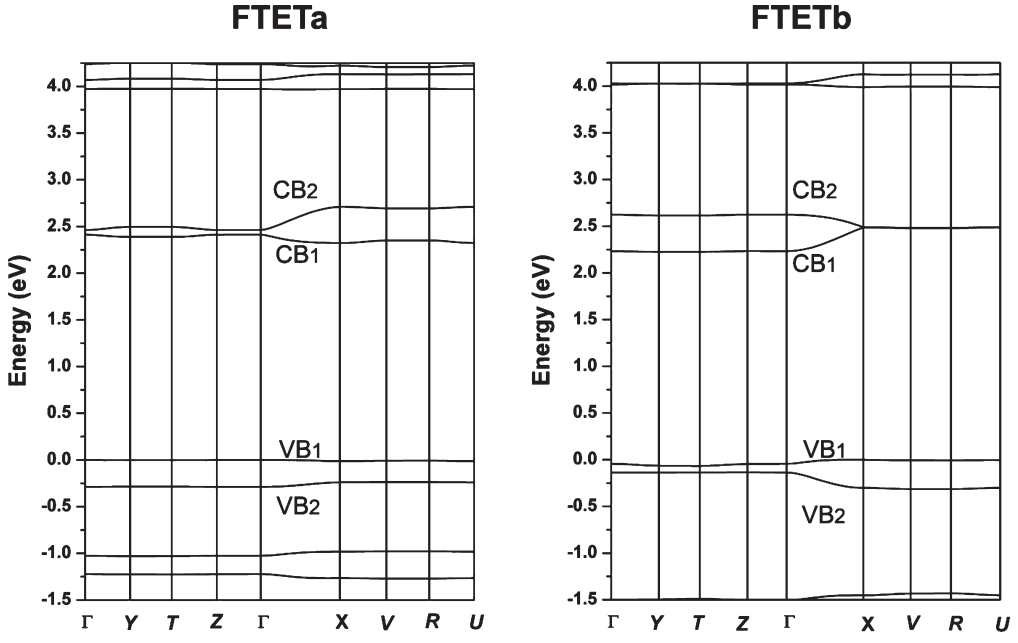

Figure 3. DFT-B3LYP/6−21G electronic band structures of the **FTETa** and **FTETb** crystals. Points of high symmetry in the first Brillouin zone are labeled as follows: Γ = (0,0,0), *Y* = (0,0.5,0), *T* = (0,0.5,0.5), *Z* = (0,0,0.5), *X* = (0.5,0,0), *V* = (0.5,0.5,0), *R* = (0.5,0.5,0.5), and *U* = (0.5,0,0.5), all in reciprocal space coordinates.

in the crystal with the electron-rich ring (alkyl/alkoxy-substituted ring) facing the electron-poor ring (fluorinated ring), which is indicative of arene-perfluoroarene interactions. As a consequence of the different relative intermolecular orientations in the a- and b-type dimers, the corresponding intermolecular wave function overlap integrals and the electronic couplings are also notably different (see Figure 2); for instance, in **FTETa**, in the case of holes, t^h = 110 meV in a-dimers and 6 meV in b-dimers.

The electronic band structures of **FTETa** and **FTETb** are shown in Figure 3 (details are given in Table S8 of the Supporting Information). In both systems, the valence band (VB) and conduction band (CB) consist of two sub-bands arising from the interaction of the HOMO and LUMO levels, respectively, of the two translationally inequivalent molecules present in the unit cell. The maximum [minimum] of the upper [lower] valence [conduction] sub-band, VB_1 [CB_1], is located at the *Z* [*X*] point in **FTETa** and *X* [*Y*] point in **FTETb**. We note, however, that because of the flatness of the bands, these *k*-states are energetically quasi-degenerate. For instance, the CB at the Γ-point in **FTETb** is located only 8 meV above the band minimum. As seen from Figure 3, both the CB and VB show a noticeable dispersion only along Γ*X* (corresponding to the direction along the π-stacks); as a result, the largest variation in the sub-band splitting, which is in general more pronounced for the CB than for the VB, is also observed along this direction.

Interestingly, the patterns of the CB of **FTETa** and **FTETb** show opposite trends. For instance, the largest band splittings in **FTETa** take place along the *X*, *V*, *R*, and *U*-points, whereas negligible splittings are observed along Γ, *Y*, *T*, and *Z*-points; in **FTETb**, however, a completely reverse trend is found.

These differences in the band structures of **FTETa** and **FTETb** can be rationalized in the framework of a tight-binding model for systems with two sites per unit cell. Because for these compounds the largest couplings are found only along the π-stacking direction, for the sake of simplicity, we can limit our discussion to the one-dimensional case. In this instance, the band energies are given by[42]

$$E(k) = \frac{\Delta_1 + \Delta_2}{2} \pm \sqrt{\left(\frac{\Delta_1 - \Delta_2}{2}\right)^2 + |L_{12}(k)|^2} \quad (1)$$

where

$$|L_{12}(k)|^2 = t_a^2 + t_b^2 + 2t_a t_b \cos k(d_a + d_b) \quad (2)$$

Here, $\Delta_i (i = 1, 2)$ represents the molecular site energy, k is the electron wave vector, and $t_{a(b)}$ denotes the transfer integral for the corresponding dimer. Equations 1 and 2 illustrate that the band splitting increases [decreases] with wave vector when transfer integrals t_a and t_b have opposite signs [the same sign]. Thus, the opposite trends in the band patterns of **FTETa** and **FTETb** are a simple consequence of the respective signs of the transfer integrals in these systems. For instance, in the case of the CB, t_a and t_b are both positive in **FTETb** while they have opposite signs in **FTETa** (see Figure 2). This simple model also explains the larger VB splitting in **FTETb** than in **FTETa**. This is related to the fact that one of the transfer integrals in **FTETa** is very small (t_a = 110 meV and t_b = 6 meV), which makes the wave-vector dependent contribution to the band splitting (third term in eq 2) insignificant. In contrast, for **FTETb**, the absolute values of the transfer integrals are comparable ($t^h = -51$ meV and t^h = 81 meV); as a result, the VB splitting significantly depends on the wave vector.

It is important to recall that charge transport along π-stacks presenting an alternation in intermolecular distances (dimerized pattern), independently of whether a hopping regime or a bandlike regime is applicable, is defined by the smaller transfer integral rather than the average of the two. For example, in the band model, a key parameter is the effective mass of the charge carriers, m_{eff}. The effective mass is related to the curvature of the band minimum/maximum; in the one-dimensional case, it reads

$$m_{eff}^{-1} = \frac{1}{\hbar^2}\frac{\partial^2 E(k)}{\partial k^2} \quad (3)$$

When the molecular site energies are the same ($\Delta_1 = \Delta_2$), eqs 1−3 yield

$$m_{eff} = \frac{\hbar^2}{2t_{eff}\left(\frac{d_a + d_b}{2}\right)^2} \quad (4)$$

$$t_{eff} = \frac{2t_a t_b}{t_a + t_b} \quad (5)$$

Here, d_a and d_b denote the intermolecular distance within the a- and b-dimer, respectively. Thus, in the case of holes in **FTETa** (t_a = 110 meV and t_b = 6 meV), although the average transfer integral is about 56 meV, the effective (reduced) transfer integral is only 11 meV; this results in an effective mass estimated from eq 4 of about 20 m_e (where m_e is the free electron mass). Thus, a dimerized stacking is likely to adversely affect the charge−transport properties.

The smallest effective mass derived from the band-structure calculations, $m_{eff} = 2.2\, m_e$, is obtained for electrons in **FTETb** along the π-stacking (Γ*X*) direction. This value is on the same order as that found in organic systems considered as good electron-transport materials, such as perfluorotetracene (2.88 m_e) and perfluoropentacene (2.08 m_e).[39]

FTETc also contains two translationally inequivalent molecules per unit cell. However, in contrast to **FTETa** and **FTETb** where both molecules are arranged in an alternating manner along 1D π-stacks, **FTETc** forms an alternating arrangement of quasi-2D planar structures (*ab*-plane, see Figure 4) where each 2D-structure consists of the same molecule. It is interesting to note that for the π-stacks along the *a*-axis, the molecules arrange in a parallel cofacial fashion with a single intermolecular separation of 3.35 Å; the moderate long-axis sliding (3.48 Å) is likely due to interactions between fluorine atoms of one molecule and the electron-poor center of a partially fluorinated ring on an adjacent molecule, as also observed in other perfluorinated aromatic compounds.[16,39] The electronic band structure of the **FTETc** crystal is shown in Figure 5. As the electronic coupling between translationally inequivalent molecules is negligible, the VB and CB are 2-fold degenerate with total bandwidths of 553 and 461 meV, respectively (see also Table S8 in the Supporting Information). These values are comparable to those in pentacene[43,44] and almost twice as large as those in rubrene (340 and 160 meV for the VB and CB widths, respectively).[38] The VB maximum is located at the *X*-point, whereas the CB minimum is found at the *V*-point (leading to an indirect gap of 2.20 eV). In the case of the VB, only the Γ*X* direction, which corresponds to the cofacial π-stacking along the *a* crystallographic axis, provides for a significant dispersion (553 meV). This result is confirmed by the direct calculations of the

(42) Liuolia, V.; Valkunas, L.; vanGrondelle, R. *J. Phys. Chem. B* **1997**, *101*, 7343.
(43) de Wijs, G. A.; Mattheus, C. C.; de Groot, R. A.; Palstra, T. T. M. *Synth. Met.* **2003**, *139*, 109.
(44) Hummer, K.; Ambrosch-Draxl, C. *Phys. Rev. B* **2005**, *72*, 205205.

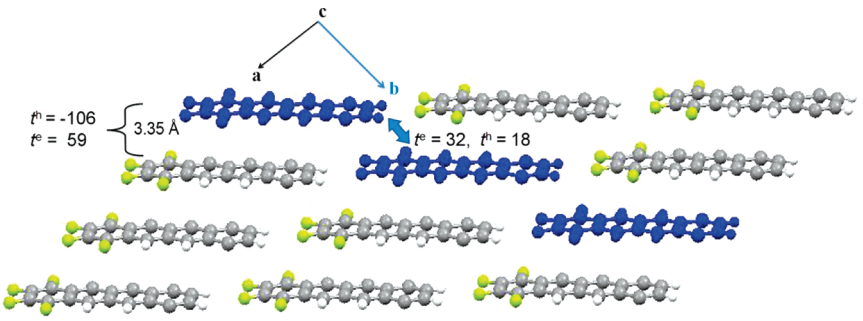

Figure 4. Crystal structure of **FTETc** viewed along the *c* direction of the crystal lattice showing the intermolecular distances between π−stacked cofacial dimers along the *a* crystallographic direction, as given in ref 18. Molecules highlighted in blue indicate the π-stacking along the *b* direction of the crystal lattice. The DFT estimates of the transfer integrals (in meV) for holes (t^h) and electrons (t^e) for specific molecular pairs are also shown.

transfer integrals for dimers, yielding a value of $t^h = -106$ meV along this π-stack (giving an estimated bandwidth of 424 meV in the framework of a one-dimensional tight-binding model, in reasonable agreement with the DFT band-structure calculations). Thus, hole transport in **FTETc** is predicted to be significant only along the *a* axis. The corresponding effective mass is estimated to be about $m_{eff}/m_e = 1.5$; this very small value is comparable with values of 1.69 m_e and 1.22 m_e for the hole effective masses derived along the π-stacking direction in the perfluorotetracene and perfluoropentacene crystals, respectively.[39] For the sake of comparison, we note that the smallest effective mass for holes in pentacene[43] is estimated to be 1.7 m_e and a value of 1.0 m_e is found in rubrene.[45]

In the case of the conduction band, the dispersion along the ΓX direction (169 meV) is significantly smaller than that for the VB. This is consistent with the smaller value of $t^e = 59$ meV calculated for a dimer. Note that in a simple 1D tight-binding model this t^e value would result in a bandwidth around ($4 \times t^e =$) 240 meV, that is significantly larger than the calculated bandwidth of 169 meV; this suggests that in this case the electronic structure cannot be simply based on a one-dimensional tight-binding model. In fact, significant dispersion (196 meV) is also found along the ΓY direction (that is, along the *b* crystal axis that runs across neighboring π-stacks, see Figure 4). Direct calculations of transfer integrals for dimers along the *b* direction are indicative of moderate electronic couplings for electrons (32 meV), see also Figure 5. Thus, electron transport has a significant two-dimensional character in the **FTETc** crystal. We note that the effective mass for electrons is estimated to be 1.9 m_e at the conduction band edge; this is even smaller than in **FTETb** and the perfluoroacenes.

Finally, we turn to the **FTETd** crystal. Its unit cell contains four translationally inequivalent molecules that can be further divided into two groups based on differences in molecular geometry. The geometry differences result in site energy differences of 17 and 2 meV for electrons and holes, respectively. As a result, the **FTETd** crystal is characterized by two geometrically inequivalent π-stacks (labeled 1 and 2 in Figure 6). Each stack contains two geometrically identical but translationally

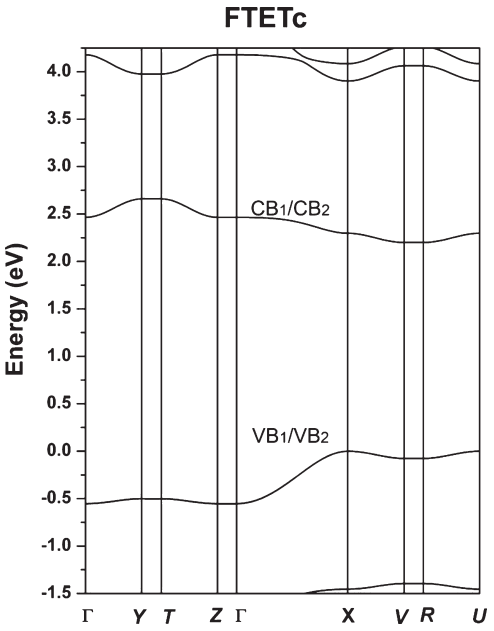

Figure 5. DFT-B3LYP/6−21G electronic band structure of the **FTETc** crystal.

inequivalent molecules, which arrange in the same manner (i.e., in an antiparallel cofacial configuration) as in the **FTETa** and **FTETb** crystals. Thus, the CB and VB of **FTETd** (Figure 7) can be viewed as a superposition of two slightly different CBs and VBs, each similar to those in the **FTETa** and **FTETb** crystals.

The band structures can again be rationalized in the framework of the tight-binding model used in the case of **FTETa** and **FTETb**. The upper valence sub-band (VB_1) is separated from the lower conduction sub-band (CB_1) by an indirect bandgap of 2.24 eV (between the *T* and Γ-points). Both valence and conduction bands of **FTETd** split into four sub-bands. The band splitting for the CB is larger than for the VB (334 vs. 130 meV at Γ; 250 vs. 111 meV at *X*, respectively); this is consistent with the larger electronic couplings calculated for the electrons (Figure 6). As in **FTETa** and **FTETb**, the strongest dispersion in both CB and VB is found along the ΓX direction; this is expected from geometry considerations and from the electronic-structure calculations, which suggest that significant electronic couplings occur only between adjacent molecules along the π-stacks.

(45) Li, Z. Q.; Podzorov, V.; Sai, N.; Martin, M. C.; Gershenson, M. E.; Di Ventra, M.; Basov, D. N. *Phys. Rev. Lett.* **2007**, *99*, 016403.

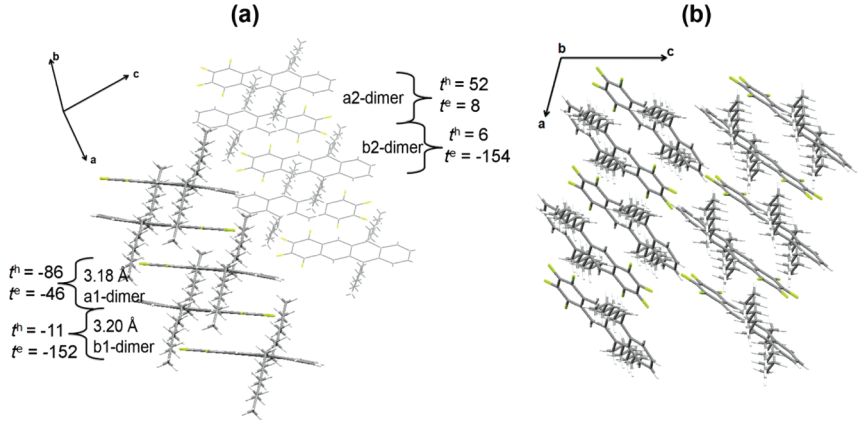

Figure 6. (a) Crystal packing (view along the short axis) of **FTETd** showing the intermolecular distances between the a- and b-type dimers for the two geometrically different π-stacks 1 (capped sticks) and 2 (wireframe).[18] The DFT transfer integrals (in meV) for holes (t^h) and electrons (t^e) for selected molecular pairs are also shown. (b) Crystal structure of **FTETd** along the *b* direction of the crystal lattice.

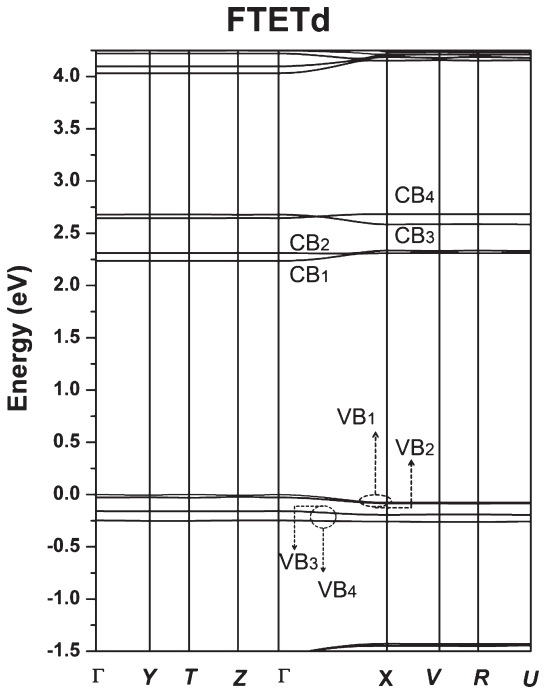

Figure 7. DFT-B3LYP/6−21G electronic band structure of **FTETd** crystal.

4. Conclusions

We have investigated the electronic structure and charge-transport parameters in four partially fluorinated tetracenes substituted with alkyl or alkoxy side chains. The results indicate that the incorporation of both donor and acceptor substituents, in comparison to tetracene, leads to a substantial increase in the geometry modifications upon both oxidation and reduction. As a result, the reorganization energies for hole transport in **FTETa**−**d** are in the range of 160−270 meV, which is two to three times larger than in tetracene. The reorganization energies for electron transport in **FTETa**−**d** are also larger by 30−60% than in **TET**. The alkoxy-substituted tetracenes (**FTETa** and **FTETb**) have higher reorganization energies than the alkyl-substituted compounds (**FTETc** and **FTETd**), which is consistent with the large geometry relaxations observed within the C−O bonds of these compounds. Among the series, **FTETc** presents the smallest reorganization energies for holes and electrons, with values nearly identical to those calculated for the partially fluorinated compounds, **FTET**; the reorganization energies in **FTETc** are smaller than those found in a good electron-transport material such as perfluoropentacene. The calculated electron affinities suggest that the electron injection barrier from a low work-function electrode is smaller than in tetracene.

The results of band-structure and transfer integral calculations point to a one-dimensional charge-transport character in all systems, except for electrons in **FTETc**, which present a 2D transport character. The largest band dispersion and consequently the smallest effective mass are obtained for holes in the **FTETc** crystal. Although the electronic couplings for holes in the **FTETa** and **FTETb** crystals are similar to those in **FTETc**, the hole effective masses are significantly higher (by 1 order of magnitude) than in **FTETc**. We have been able to show that this is a consequence of the dimerization pattern observed in the alkoxy-substituted crystals.

Overall, among the series investigated in this work, the **FTETc** crystal appears as the most promising material with regard to charge-transport properties: (i) it presents the smallest local electron−phonon couplings for both holes and electrons; (ii) the valence bandwidth is large (0.55 eV) and, accordingly, the effective mass of the hole is low (1.5 m_e); and (iii) electron transport has a 2D character and the electron effective mass ($\sim$1.9 m_e) is calculated to be lower than in the perfluoroacenes. At this point in time, however, we are unaware of any measurements of charge mobilities in these crystals. We hope that the present results can stimulate work in these directions.

Acknowledgment. This work has been supported by the National Science Foundation, primarily through the MRSEC Program under Award Number DMR-0819885 and partly through the STC Program under Award Number DMR-0120967. M.C.R.D. thanks the Spanish Ministry of Education and Science (MEC) for a MEC/Fulbright Postdoctoral Fellowship at the Georgia Institute of Technology.

We are grateful to T. Swager and D. A. da Silva Filho for helpful discussions.

Supporting Information Available: B3LYP/6-31G(d,p) bond lengths for the optimized neutral and ionic states of **FTETa**−**d**, **TET**, and **FTET** (Tables S1−S6); B3LYP/6-31G(d,p) dipole moments in **FTETa-d** and **FTET** (Table S7); calculated bandwidths for the **FTETa-d** crystals along the Γ*X* direction (Table S8) (PDF). This material is available free of charge via the Internet at http://pubs.acs.org.